Graph Regularized EEG Source Imaging with in-Class Consistency and out-Class Discrimination

Feng Liu, Jay Rosenberger, Yifei Lou, Rahilsadat Hosseini, Jianzhong Su, Shouyi Wang*

Abstract—EEG source imaging integrates temporal and spatial components of EEG to localize the generating source of electrical potentials based on recorded EEG data on the scalp. As EEG sensors can't directly measure activated brain sources, many approaches were proposed to estimate brain source activation pattern given EEG data. However, since most part of the brain activity is composed of the spontaneous non-task related activations, true task caused activation sources will be corrupted in strong background signal. For decades, the EEG inverse problem was solved in an unsupervised way without any utilization of the label information that represents different brain states. We propose that by leveraging label information, the task related discriminative sources can be much better retrieved among strong spontaneous background signals. A novel model for solving EEG inverse problem called Laplacian Graph Regularized Discriminative Source Reconstruction which aims to explicitly extract the discriminative sources by implicitly coding the label information into the graph regularization term. The proposed model can be generally extended with different assumptions. The extension of our framework is applied to VB-SCCD model which aim to estimate extended brain sources by including a spatial total variation regularization term. Simulated results show the effectiveness of the proposed framework.

Index Terms—EEG Source Imaging, Inverse Problem, Discriminative Source, Graph Regularization, Sparse Representation

1 Introduction

Due to its low cost, easy portability, high temporal resolution, and no exposure to radioligands, electroencephalography (EEG) has become one of the most popular brain imaging tools. Compared to other techniques such as positron emission tomography (PET) and functional magnetic resonance imaging (fMRI), EEG is a direct measurement of real-time electrical neural activities, and EEG is more suitable to answer exactly *when* different brain modules are activated and hence in what processing steps each module is involved [1]. PET and fMRI cannot be used to assess rapidly varying neuronal activity due to the slow response of metabolism [2]. Successful applications of EEG can be found in several clinical environments, such as real-time monitoring of patients' sleep apnea [3], detection and prediction of epilepsy seizures [4] [5].

As the EEG electrodes measure electrical activities on the scalp surface instead of directly measuring the active neurons in the brain, it doesn't provide conclusive locations and distributions of the related activated sources, which attracts more interests among neuroscientists. The problem of inferring the brain source from the recorded EEG is termed as the *inverse problem*. Solving the inverse problem can facilitate the understanding how our brain is functioning under different cognitive tasks, and the discovery of underlying reason that caused brain functionality impairment as suffered by patients with neurological disorders such as Parkinson's and Alzheimer's disease. Precise localization of activated sources inside the brain can offer an insightful awareness of the responsible cortex regions that collaborated to perform certain cognitive tasks. Contrary to the *forward problem*, which consists of modeling the contribution of each voxel to the EEG sensors by solving Maxwell's equation, the inverse problem is ill-posed since the number of interior brain voxels being considered is far greater than the number of sensors outside the scalp. To precisely estimate the responsible sources of EEG activity from at least several thousands of potential contributing locations that are distributed across the brain requires prior knowledge or assumption. Mathematically speaking, in order to find a unique solution for the ill-posed problem, constraints or assumptions have to be incorporated. Provided with different neurophysiological assumptions regarding the structure of possible source configurations [6], the goal is to find a unique and stable solution that best explains the data we observed in the EEG channels. One of the earliest commonly used priors for EEG source reconstruction is based on the ℓ_2 norm, known as the minimum norm estimate (MNE) inverse solver [7]. This MN inverse solver leads to a minimum norm estimates (MNE) of the sources. However, ℓ_2-based solvers always give a diffuse solution, resulting in an overestimation of the number of factually activated sources. Other assumptions or priors are presented in different inverse algorithms, such as, MUltiple SIgnal Classifier (MUSIC) and Recursively Applied and Projected MUSIC (RAP MUSIC) [8] [9], which adopted a spatiotemporal independent topographies (IT) model with recursive subspace projection; low resolution brain electromagnetic tomography (LORETA) [10] and standardized LORETA [11], which enforces spatial smoothness of the source located on neighboring voxels, FOCal Underdetermined

- *F. Liu, J. Rosenberger, R. Hosseini, S. Wang are with the Department of Industrial, Manufacturing, and Systems Engineering at The University of Texas at Arlington, Arlington, TX, USA.*
- *Y. Lou is with Department of Mathematical Sciences at Univeristy of Texas at Dallas, Richardson, TX, USA.*
- *J. Su is with Department of Math at Univeristy of Texas at Arlington, Arlington, TX, USA.*
  E-mail: {feng.liu, rahilsadat.hosseini}@mavs.uta.edu, {jrosenbe, su, shouyiw,}@uta.edu, yifei.lou@utdallas.edu.
- *S. Wang is the corresponding author.*

Manuscript received date xxxx

System Solution (FOCUSS) [12], which combines the advantages of distributed dipole modeling and linear estimation methods by allowing current sources to take arbitrary shape with high resolution; weighted minimum norm-LORETA (MNE-LORETA) [13], which make compensates deeper sources; dynamic Maximum Posterior Expectation-Maximization (dMAP-EM) source localization algorithm, which uses the prior knowledge that cortical activation is a distributed spatiotemporal dynamic process supported by local and long-distance neuroanatomic connections [14]; Bernoulli-Laplace priors, which introduced $\ell_0 + \ell_1$ norm in a Bayesian framework [15]; Mixed Norm Estimates (MxNE), which imposes sparsity over space and smoothness over time using $\ell_{1,2}$-norm regularization [16] [17]; Solution Space Sparse Coding Optimization (3SCO) [18], which is based on particle swarm optimization and an ℓ_0 constraint; graph Fractional-Order Total Variation (gFOTV) [19], which impose sparsity of the spatial fractional derivatives so that it locates source peaks by providing the freedom of choosing smoothness order. Recently, it is found that the enforcement of sparseness in the original domain can be an insufficient estimation of source extents, extended patches of activated source can be obtained by enforcing sparseness in transformed domains [20] [21] [22].

As summarized above, based on different assumptions or prior knowledge, different algorithms solving the inverse problem were proposed. It's worth noting that all the EEG inverse problem solvers solve the problem in an unsupervised way without taking any available label information. According to previous research [23] [24], most of the EEG signal originates from the brains spontaneous behavior, while the task related activation energy is not as strong, which rationalized the utilization of label information. The remaining question is how to fuse the label information into the traditional EEG inverse model that can explain the data well and find the discriminative activation pattern? We develop a novel model with graph regularization that implicitly uses the label information with the capability to promote in-class consistency and out-class discrimination, so that we can eradicate the spurious noise and find the different activation patterns for different classes. To solve the problem, we find in literature that the similar formulation has been addressed in the computer vision community, but we tailor the algorithm to solve our proposed model and EEG inverse problem. Usually, when we design a sequence of experiments to record the EEG and asked the subjects to perform different psychological tasks within certain time windows, the label information (happiness, sadness, surprise, etc. in emotion processing experiment, or different motion imagination tasks in brain computer interface (BCI) studies) of the recorded EEG data can be easily obtained. We implemented the graph regularized version of discriminative source reconstruction, tested on simulated EEG data, and showed its effectiveness in finding the discriminative sources and precision localization of the task-related sources.

The contributions of this paper are listed as follows: (1) We propose to use label information to solve the EEG inverse problem in a supervised way. (2) A graph regularized EEG inverse model is presented that can promote in-class consistency and out-class discrimination. (3) A Voting Orthogonal Matching Pursuit algorithm is given to decompose the common sources. (4) The extension of our proposed framework is illustrated in a transformed domain and an alternating direction method of multipliers (ADMM) based algorithm is given to solve it.

2 The Inverse Problem

Under the quasi-static approximation of Maxwell's equations, the measured EEG signal X can be described as the following linear function of current sources S,

$$X = LS + E, \tag{1}$$

where $X \in \mathbb{R}^{N_c \times N_t}$ is the EEG data measured at a set of N_c electrodes for N_t time points, $L \in \mathbb{R}^{N_c \times N_s}$ is the lead field matrix, which maps the brain source signal to sensors on the scalp, each column of L represents the activation pattern of a particular source to the EEG electrodes. Fig.1 gives an exemplary brain model. The cortex is represented with triangle meshes; each triangle represents a brain voxel. In this paper, we use the brain model and lead field matrix interchangeably. In addition, we use the terms brain voxel, source, and dipole interchangeably, sometimes using triangle as well. The number of triangles is equal to N_s. $S \in \mathbb{R}^{N_s \times N_t}$ represents the corresponding electrical potentials in N_s source locations for all the N_t time points. $E \in \mathbb{R}^{N_c \times N_t}$ is an additive noise signal. As L is a matrix in which the number of columns far exceeds the number of rows, the inverse problem is ill-posed. To seek a unique solution, a regularization term has to be adopted. An estimate of S can be found by minimizing the following cost function, which is composed of a data fidelity term and a regularization term:

$$\arg\min_S \|X - LS\|_F^2 + \lambda\Theta(S). \tag{2}$$

The regularization term $\Theta(S)$ discourages complicated source configurations temporally or spatially and enforces neurophysiologically plausible solutions, and $\|\cdot\|_F$ is the Frobenius Norm. The regularization term usually take the form of ℓ_2, ℓ_1, or a mixed norm [16] [17], spatially smooth formulation such as in LORETA algorithm or spatial total variation formulation in a transformed domain [21]. One of the most intuitive formulations is to use ℓ_0-norm to restrict the total number of activated sources less than a scalar k; the following formulation can be used:

$$\arg\min_S \|X - LS\|_F^2 \qquad s.t.\ \|s_i\|_0 \leqslant k, \tag{3}$$

Since the ℓ_0-norm constrained problem is NP-hard, approximating ℓ_0 with ℓ_1-norm is a common practice. Donoho suggested that ℓ_1 and ℓ_0 norm are equivalent under certain conditions [25]. The ℓ_1-norm regularized formulation is described as

$$s_i = s^*(x_i, L) = \arg\min_{s_i} \|x_i - Ls_i\|_2^2 + \gamma\|s_i\|_1. \tag{4}$$

The ill-posed problem of Eq.1 arises from the fact that the L is a wide matrix, and the number of columns is greater than the number of rows. From a linear system perspective, the dimension of the observed output is less than that of the input signal, making inferring s_i from x_i an under-determined problem with infinite solutions if no regularization term is applied. Given the EEG recordings at a time point, which is denoted as the ith column, x_i, of the X matrix, we want to represent the signal with minimum error by trying to find the best linear representation from activation patterns (atoms) in the over-complete dictionary L. The solution s_i is the sparse coding for the x_i in the dictionary L, the non-zero entries in s_i represent the activated regions inside the brain.

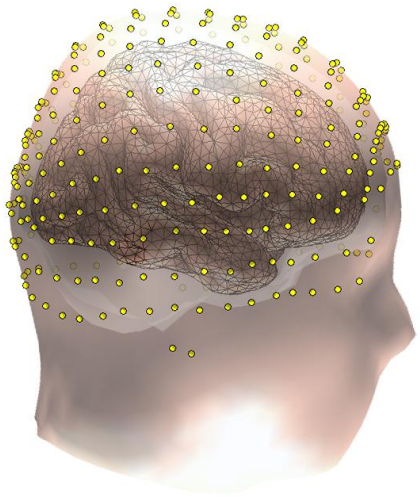

Fig. 1: Triangle meshed realistic brain model. Each triangular element represents a current dipole located at its center, and the orientation of dipoles is assume to be perpendicular to the cortical surface.

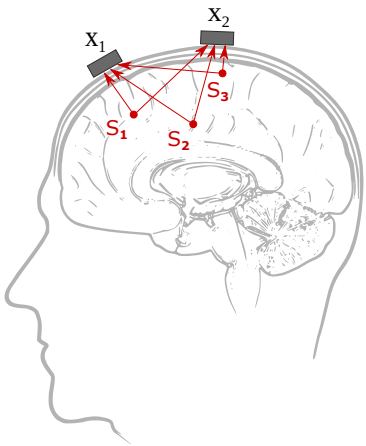

Fig. 2: Sources propagate to electrodes: s_3 is the common activation source and has larger magnitude, s_1 is a discriminative source corresponding to class 1, and s_2 is a discriminative source corresponding to class 2.

3 Proposed Framework

3.1 Discriminative Source Reconstruction with Graph Regularization

According to previous research [23] [24], most the EEG potentials originate from the non-task related spontaneous neural firing that can be regarded as the background activity. Combined with the fact that an EEG signal is non-stationary with low SNR, traditional method is hard to extract discriminative signal of interests. A simple example is shown in Fig.2, s_1 and s_2 represent the discriminative sources corresponding to class 1 and class 2, s_3 is the common source shared by class 1 and class 2. If the magnitude of s_3 is much larger than s_1 and s_2, a lot of algorithms will fail to infer the discriminative sources under low SNR. In the following numerical experiments section of this paper, we use similar source configurations: each class has a dominant primary source that is shared with other classes and relatively small secondary source that is unique to this class. We are trying to get consistent inverse solutions under the same brain state and discriminative solutions given different brain states utilizing the available label information. Inspired by the successful applications of graph regularization in computer vision community [26] [27], the proposed model is in the form of sparse representation of discriminative sources with a graph regularization term, which is termed as Laplacian Graph Regularized Discriminative Source Reconstruction (LGRDSR), and includes the source reconstruction fidelity term and label guided in-class consistency and out-class discrimination term:

$$\begin{aligned}\langle S\rangle = &\arg\min_{S} \|X - LS\|_F^2 + \alpha\|S\|_{1,1} \\ &+ \frac{\beta}{2}\sum_{i,j=1}^{N}\|s_i - s_j\|_2^2 M_{ij},\end{aligned} \tag{5}$$

where $X \in \mathbb{R}^{N_c \times N}$, N is the total number of time points from different classes, $\|\cdot\|_{1,1}$ is the ℓ_1 norm notation for a matrix, equal to the sum of the absolute values of all elements in a matrix, the second term is the cost of sparse coding, and the third term is the graph regularization term that requires the sources within the same category to have similar patterns while making the sources for different classes to be distinct. The definition of the M matrix is written as:

$$M_{ij} = \begin{cases} +1, & \text{if } (s_i, s_j) \text{ belong to the same class} \\ -1, & \text{if } (s_i, s_j) \text{ belong to different classes} \end{cases}$$

The goal of this formulation is to find discriminative sources while maintaining the consistency of in-class reconstructed sources.

Remarks on *design of M matrix*

When (s_i, s_j) belong to the same class, the value of M_{ij} should be positive, which will penalize difference in in-class sources. By driving the intrinsic geometric structure of s_i and s_j to be the same, the in-class consistency of the sources can be achieved.

When (s_i, s_j) belong to different classes, assigning a negative value to M_{ij} will explicitly promote out-class discrimination of the source. In practice, if we care more about in-class consistency, we can set $M_{ij} = 0$ when (s_i, s_j) belongs to different classes. The magnitude of M_{ij} can also be adjusted to tailor the relative weight between in-class consistency and out-class discrimination.

Define D as a diagonal matrix whose entries are column or row sums of the symmetric matrix M, $D_{ii} = \sum_j M_{ij}$, define $G = D - M$, where G is called the graph Laplacian Matrix [27], The third term of Eq.5 can be further derived as:

$$\begin{aligned}\sum_{i,j=1}^{N}\|s_i - s_j\|_2^2 M_{ij} &= \sum_{i,j=1}^{N}({s_i}^T s_i + {s_j}^T s_j - 2{s_i}^T s_j)M_{ij} \\ &= 2tr(SGS^T).\end{aligned}$$

As a result, Eq.5 is written as

$$\begin{aligned}\langle S\rangle = &\arg\min_{S} \|X - LS\|_F^2 + \alpha\|S\|_{1,1} \\ &+ \beta(Tr(SGS^T)).\end{aligned} \tag{6}$$

Eq.6 can be rewritten into a decomposed form

$$\begin{aligned}\langle s_1, s_2, \ldots s_N\rangle = &\arg\min_{s_1,s_2,\ldots s_N} \sum_{i=1}^{N}\|x_i - Ls_i\|_2^2 \\ &+ \beta\sum_{i,j=1}^{N} G_{ij} s_i^T s_j + \alpha\sum_{i=1}^{N}\|s_i\|_1.\end{aligned} \tag{7}$$

Fixing the other sources s_j ($j \neq i$) while solving s_i, each problem is presented as

$$\begin{aligned}\langle s_i \rangle = &\arg\min_{s_i} \|x_i - Ls_i\|_2^2 + \beta G_{ii} s_i^T s_i \\ &+ s_i^T h_i + \alpha \sum_{k=1}^{N_s} \left| s_i^{(k)} \right|,\end{aligned} \tag{8}$$

where $h_i = 2\beta(\sum_{j\neq i} G_{ij}s_j)$, and $s_i^{(k)}$ is the k-th coefficient of vector s_i. Eq.8 can be solved using feature-sign search algorithm [28] [27] [29]. To better describe the feature-sign search algorithm, denote $g(s_i) = \|x_i - Ls_i\|_2^2 + \beta G_{ii} s_i^T s_i + s_i^T h$ and $f(s_i) := g(s_i) + \alpha \sum_{k=1}^{N_s} \left| s_i^{(k)} \right|$, Eq.8 is rewritten as $\langle s_i \rangle = \arg\min_{s_i} f(s_i) = \arg\min_{s_i} g(s_i) + \alpha \sum_{k=1}^{N_s} \left| s_i^{(k)} \right|$. Each s_i is solved sequentially while fixing other s_j ($j \neq i$). Algorithm (1) presented the famous feature-sign search algorithm properly adapted for Eq.6 with the graph regularized term. Note that the analytical solution for Eq.8 is $\tilde{s}_i^{new} = (L^T L + \beta G_{ii} I)^{-1}(\tilde{L}^T x_i - \frac{\alpha\tilde{\theta} + \tilde{h}_i}{2})$ in part b) of the feature-sign stage of Algorithm (1), and the inversion of $L^T L + \beta G_{ii} I$ is the most computationally expensive part since L matrix is overdetermined wide matrix, the calculation speed can be boosted by using *Woodbury formula* [30]:

$$(L^T L + \beta G_{ii} I)^{-1} = \frac{1}{\beta G_{ii}}(I - \frac{1}{\beta G_{ii}} L^T (LL^T + \frac{1}{\beta G_{ii}} I)^{-1} L).$$

The inverse operation of a matrix with the same dimension as the number of dipoles/voxels is reduced to the inverse of a matrix with the dimension number equal the total number of electrodes, as a result, the calculation cost is reduced significantly. Different from original version of feature sign search algorithm which includes only the inner for-loop, Algorithm (1) has an while-loop since the updates of all $s_j (j \neq i)$ will impact the solution of s_j due to the inclusion of graph regularized term, the algorithm stops until the convergence of S^*.

3.2 Common Sources Decomposition with Voting Orthogonal Matching Pursuit (VOMP)

Under the assumption of strong common spontaneous source activation pattern, the contribution of discriminative sources to the EEG recorded data is relatively small, making the solution space for different classes highly correlated, which limits the capability of discrimination. Previous research has shown that pulling out the high absolution value of coefficients s_{ij} associated with the common activation pattern can assist to find the discriminative source of interest [31].

In the similar way as addressing the "cross-and-bouquet" model presented in [32], a useful step is decomposition of X for better extraction of discriminative sources. Similar procedure can be found in [33]. As we assumed, the spontaneous source activation pattern is very strong, thus making the convex hull spanned by all the source configuration to a tiny portion of the space [32]. The Voting Orthogonal Matching Pursue (VOMP) is proposed as given in Algorithm 2. The aim is to extract the common sources across all classes by voting the most popular source location using stepwise orthogonal matching pursuit. Problem (9) describes the common source decomposition problem. The VOMP is considered as an integral preprocessing part to find discriminative sources. The procedure to solve Problem (6) is given in Algorithm (3) and is illustrated in Fig.3.

$$\begin{aligned}\langle S_c \rangle = &\arg\min_{W_c} \|X - LS_c\|_F^2 \\ &s.t.\ \|s_i\|_0 \leqslant T_{max}, \quad i = 1, 2, ...N_d \\ &s_i = s_j, i = 1, 2, ...N_d, j = 1, 2, ...N_d\end{aligned} \tag{9}$$

After the decomposition of common source, its contribution to the EEG data X is also removed. The new EEG data after removal of the common source is written as $X_{new} = X - LS_c$. In the following part, we still use X to represent X_{new} when no confusion is caused.

Algorithm 3 Proposed framework of solving Problem (6)

INPUT: Lead field matrix L, EEG data X, graph matrix G
OUTPUT: Discriminative source S_d
Initialization: $T \leftarrow 1$, $\Omega = \emptyset$, $R = X$, $R_{new} = X$, $S' = 0$

while stopping criteria not met **do**
(1) Use VOMP algorithm for common source decomposition.
(2) Solve the following sparse coding problem for $\langle S \rangle = \arg\min_S \|X - LS\|_F^2 + \alpha\|S\|_{1,1} + \beta(Tr(SGS^T))$ using the feature-sign search algorithm described in Algorithm (1) .
(3) Adjust the voting threshold p.
end while

4 Extensions of Our Framework

4.1 Graph regularized sparse model with total variation constraints

We show the proposed framework can be incorporated with other states of art algorithms. The recently proposed algorithms in Ref. [21] [31] [22] are used as an example. The algorithm proposed in Ref. [31] is referred as SVB-SCCD, which adds ℓ_1 sparsity constraints to VB-SCCD algorithm proposed in [21], and Ref. [22] reconstructed extended brain sources by enforcing both variation and wavelet transformed sparsity. The key component for the above-mentioned algorithms is the total variation constraint used as a regularization term. The underlying neurophysiological reason is that the activated source is not discrete on the cortex, they should form a spatially continuous patch that all the neighboring voxels should have the same activation pattern. In this session, we choose Ref. [31] as an exemplary extension of our proposed algorithm, as VB-SCCD can be viewed as a relaxation of SVB-SCCD. Ref. [22] has an extra wavelet domain regularization term and can be similarly solved with variable splitting technique. The measurement of spatial total variation is achieved using a linear transform matrix V, defined as

$$V = \begin{bmatrix} v_{11} & v_{12} & \cdots & v_{1N} \\ v_{21} & v_{22} & \cdots & v_{2N} \\ \vdots & \vdots & \ddots & \vdots \\ v_{P1} & v_{P1} & \cdots & v_{PN} \end{bmatrix}$$

with

$$\begin{cases} v_{ij} = 1; v_{ik} = -1; & \text{if element } j,k \text{ share edge } i\ ; \\ v_{ij} = 0; & \text{otherwise.} \end{cases}$$

where $p = 1, ..., P, d = 1, ..., D$, where P is the number of edges of the triangular grid, N is the number of voxels. The VS describes the differences in amplitude between adjacent dipoles,

Algorithm 1 Feature-sign search algorithm

INPUT: Lead field matrix L, EEG data X, graph matrix G, parameter α and β
OUTPUT: Source matrix S
while S^* is not converged
for $i = 1, \ldots, N$
1. Initialization:
$s_i := \overrightarrow{0}$, $\theta := 0$, *active set* $\mathcal{A} := \{\}$, where $\theta_j \in \{-1, 0, 1\}$ denotes $\text{sign}(s_i^{(j)})$
2. Update of the active set:
For all zero coefficients of s_i, find $j = \arg\max_j |\frac{\partial g(s_i)}{\partial s_i^{(j)}}|$, add j to the *active set* $\mathcal{A}$ only if it locally improves the objective, under the following conditions:
if $\frac{\partial g(s_i)}{\partial s_i^{(j)}} > \alpha$, then let $\theta_j := -1$, $\mathcal{A} = \mathcal{A} \cup \{j\}$.
if $\frac{\partial g(s_i)}{\partial s_i^{(j)}} < -\alpha$, then let $\theta_j := 1$, $\mathcal{A} = \mathcal{A} \cup \{j\}$.
3. Feature-sign step
a) Let $\tilde{L}$ be a submatrix of L that contains only the columns corresponding to the *active set* $\mathcal{A}$, $\tilde{s}_i$ and $\tilde{h}_i$ is the subvectors of s_i and h_i similarly defined.
b) The analytical solution for Eq.8 is derived:
$\tilde{s}_i^{new} = \frac{1}{\beta G_{ii}}(I - \frac{1}{\beta G_{ii}} L^T (LL^T + \frac{1}{\beta G_{ii}} I)^{-1} L(\tilde{L}^T x_i - \frac{\alpha\tilde{\theta} + \tilde{h}_i}{2})$.
c) Perform discrete line search from $\tilde{s}_i^{new}$ to $\tilde{s}_i$:
Examine the objective value at $\tilde{s}_i^{new}$ and all points where any coefficient changes sign.
Update $\tilde{s}_i$ (and corresponding entries in s_i) where the objective function achieves the lowest value.
Remove the zero coefficients of $\tilde{s}_i$ from the *active set* and update $\theta = sign(s_i)$.
4. Check the optimality conditions
a) Optimality condition for nonzero coefficients: $|\frac{\partial g(s_i)}{\partial s_i^{(j)}}| + \alpha \text{sign}(s_i^{(j)}) = 0$, for all $s_i^{(j)} \neq 0$.
If condition (a) is not satisfied, go to step 3 to perform discrete line search.
b) Optimality condition for zero coefficients: $|\frac{\partial g(s_i)}{\partial s_i^{(j)}}| < \alpha$, for all $s_i^{(j)} = 0$.
If condition (b) is not satisfied, got to Step 2; otherwise return s_i as the solution, denoted as s_i^*
end for
end while

which give rises to the VB-SCCD optimization cost function [21], as follows:

$$\min_S \|X - LS\| + \lambda \|VS\|_{1,1}.$$

In order to imposes sparsity in the original source domain, Becker et al [31] proposed the following model called SVB-SCCD which is given below:

$$\langle S \rangle = \min_S \|X - LS\| + \lambda \|VS\|_{1,1} + \alpha \|S\|_{1,1}.$$

VB-SCCD is a special case when α is zero in SVB-SCCD model. We showed that our graph regularized framework can be incorporated in SVB-SCCD as described below,

$$\begin{aligned} \langle S \rangle = &\min_S \|X - LS\| + \lambda \|VS\|_{1,1} + \alpha \|S\|_{1,1} \\ &+ \beta (Tr(SGS^T)), \end{aligned} \tag{10}$$

which can be reformulated as

$$\begin{aligned} &\min_S \|X - LS\| + \lambda \|Y\|_{1,1} + \alpha \|Z\|_{1,1} + \beta (Tr(SGS^T)) \\ &s.t. \quad Y = VS, \quad Z = S. \end{aligned} \tag{11}$$

We name the above model Graph regularized version of SVB-SCCD (GSVB-SCCD), which considers the sparsity in both original source space and transformed space, as well as the in-class consistency and out-class discrimination capability imposed by the graph regularization term. The new formulation makes the objective function separable with respect to three variables S, Y and Z. For Problem (11), S can also be decomposed as

$$\begin{aligned} &\min_{s_i} \|x_i - Ls_i\|_2^2 + \lambda \|y_i\|_1 + \alpha \|z_i\|_1 + \beta G_{ii} s_i^T s_i + s_i^T h_i \\ &s.t. \quad y_i = Vs_i, \quad z_i = s_i. \end{aligned} \tag{12}$$

4.2 ADMM Algorithm

Problem (12) can be attacked using alternating direction method of multipliers (ADMM) [34] after forming it to unconstrained augmented Lagrangian function:

$$\begin{aligned} L_p(s_i, y_i, z_i, u_i, w_i) = &\|x_i - Ls_i\|_2^2 + \lambda \|y_i\|_1 \\ &+ \alpha \|z_i\|_1 + \beta G_{ii} s_i^T s_i + s_i^T h_i \\ &+ u_i^T (y_i - Vs_i) + w_i^T (z_i - s_i) \\ &+ \frac{\rho}{2} \|y_i - Vs_i\|_2^2 \\ &+ \frac{\rho}{2} \|z_i - s_i\|_2^2 . \end{aligned} \tag{13}$$

Augmented Lagrangian methods can bring robustness to the solution compared to other penalty. The variable s_i, y_i, z_i, u_i,w_i are updated sequentially, with the hope that each subproblem has a closed form solution or can be calculated efficiently. In short,

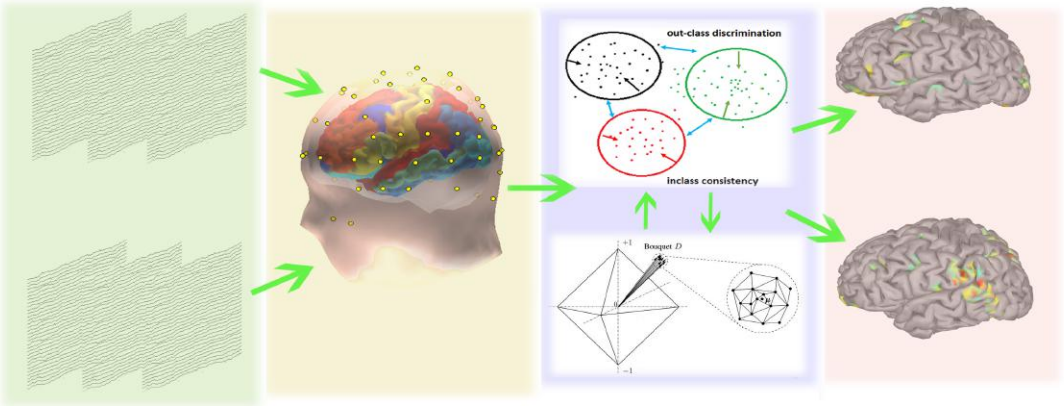

Fig. 3: Procedures of our framework: After gathering labeled EEG recorded data, the brain model is constructed using finite element method (BEM) based on MRI images, then we first use the VOMP algorithm to decompose the primary common source starting with a high minimum voting percentage, and then solve it using feature-sign search algorithm, validate the source configurations and do these steps alternative until solutions are converged, the last step is to map discriminative sources to the cortex.

Algorithm 2 Decomposition of Non-discriminative Sources with VOMP

INPUT: Lead field matrix L, EEG data X, maximum number of common sources T_{max}, minimum voting acceptance threshold p
OUTPUT: S_c, result of removed common sources X_{new}
Initialization: $T \leftarrow 1$, $\Omega = \emptyset$, $R = X$, $R_{new} = X$, $S' = 0$

```
while Stopping criteria is not met do
    for i ∈ 1, ..., N_t do
        s_i ← OMP(L, x_i, 1)
        q_i ← nonzero index of s_i
    end for
    q_best ← most frequent q_i
    if T = T_max or frequency of f(q_best) < p then
        break;
    else
        Ω ← Ω ∪ q_best ; L' = (L_{:,i} | i ∈ Ω) ; S' ← pinv(L')X;
        S' ← mean(S'); R_new ← X − L'S'
    end if
    for k ∈ 1, ..., C do
        R^k_new = {R_new(i) | i ∈ class k} ;
        R^k = {R(i) | i ∈ class k}
    end for
    if ||R^k_new|| < ||R^k|| for k ∈ 1, ..., C then
        continue;
    else break;
    end if
    T ← T + 1; R ← R_new
end while
X_new = R_new; S_c = S'
return S_c, X_new
```

ADMM consists of five substeps, given in Eq.14 to Eq.18,

$$s_i^{(k+1)} := \arg\min_s L_\rho(s, y_i^{(k)}, z_i^{(k)}) = \arg\min_s \|x_i - Ls\|_2^2 + \beta G_{ii} s^T s + s^T h_i + \frac{\rho}{2}\left\| y_i^{(k)} - Vs + \frac{u_i^{(k)}}{\rho}\right\|_2^2 + \frac{\rho}{2}\left\| z_i^{(k)} - s + \frac{w_i^{(k)}}{\rho}\right\|_2^2 \quad (14)$$

$$y_i^{(k+1)} := \arg\min_y L_\rho(s_i^{(k+1)}, y, z_i^{(k)}) = \arg\min_y \lambda\|y\|_1 + \frac{\rho}{2}\left\| y - Vs_i^{(k+1)} + \frac{u_i^{(k)}}{\rho}\right\|_2^2 \quad (15)$$

$$z_i^{(k+1)} := \arg\min_z L_\rho(s_i^{(k+1)}, z, w_i^{(k)}) = \arg\min_z \alpha\|z\|_1 + \frac{\rho}{2}\left\| z - s_i^{(k+1)} + \frac{w_i^{(k)}}{\rho}\right\|_2^2 \quad (16)$$

$$u_i^{(k+1)} := u_i^{(k)} + \rho(y_i^{(k+1)} - Vs_i^{(k+1)}) \quad (17)$$

$$w_i^{(k+1)} := w_i^{(k)} + \rho(z_i^{(k+1)} - s_i^{(k+1)}) \quad (18)$$

The update of $s_i^{(k+1)}$ has a closed form solution, which is

$$s_i^{(k+1)} = P^{-1}[2L^T x_i - h_i + \rho V^T(y_i^{(k)} + \frac{u_i^{(k)}}{\rho}) + \rho(z_i^{(k)} - w_i^{(k)})],$$

where $P = 2L^TL + 2\beta G_{ii} I + \rho(V^TV + I)$. The inverse of P matrix is not obviously applicable to *Woodbury formula*. However, it can be addressed by solving linear systems using backward/forward substitution using Cholesky decomposition [19]. The update of $y_i^{(k+1)}$ can use the property of proximal operator in the ℓ_1 norm. Denote the ℓ_1 norm proximal operator as

$$\text{prox}_\mu(v) = \arg\min_x \mu\|x\|_1 + \frac{1}{2}\|x - v\|_2^2, \quad (19)$$

with $\mu > 0$. The above problem (19) has a closed form solution, called soft thresholding, defined by a shrinkage function,

$$\text{shrink}(v, \mu) = (|v| - \mu)_+ \,\text{sgn}(v),$$

where $(x)_+$ is x when $x > 0$, otherwise 0. The shrinkage function is efficient to solve ℓ_1 minimization problem due to its calculation is element-wise. As a result, the updates of $y_i^{(k+1)}$ and $z_i^{(k+1)}$ can be expressed as:

$$y_i^{(k+1)} = \text{shrink}(Vs_i^{(k+1)} - \frac{u_i^{(k+1)}}{\rho}, \frac{\lambda}{\rho}),$$

$$z_i^{(k+1)} = \text{shrink}(s_i^{(k+1)} - \frac{w_i^{(k+1)}}{\rho}, \frac{\alpha}{\rho}).$$

The procedure for solving problem (10) is summarized in Algorithm (4). The update of all s_i is the most time consuming, however the computation of all s_i can be submitted to distributed machines for parallel computing as it doesn't need to wait the results from other samples in the present iteration.

Algorithm 4 ADMM framework for solving problem 10

INPUT: Lead field matrix L, preprocessed EEG signal matrix X, Graph matrix G, variation matrix V, parameter α and β, λ
OUTPUT: Source matrix S
while S^* is not converged
for $i = 1, \ldots, N$
Alternating update until converge:

$$s_i^{(k+1)} = P^{-1}[2L^T x_i - h_i + \rho V^T(y_i^{(k)} + \frac{u_i^{(k)}}{\rho}) + \rho(z_i^{(k)} - w_i^{(k)})],$$
$$y_i^{(k+1)} = \text{shrink}(Vs_i^{(k+1)} - \frac{u_i^{(k+1)}}{\rho}, \frac{\lambda}{\rho}),$$
$$z_i^{(k+1)} = \text{shrink}(s_i^{(k+1)} - \frac{w_i^{(k+1)}}{\rho}, \frac{\alpha}{\rho}).$$
$$u_i^{(k+1)} := u_i^{(k)} + \rho(y_i^{(k+1)} - Vs_i^{(k+1)})$$
$$w_i^{(k+1)} := w_i^{(k)} + \rho(z_i^{(k+1)} - s_i^{(k+1)})$$

end for
end while

5 Numerical Results

5.1 Experiment setup

We used a recently developed realistic head model called ICBM-NY or "New York Head" [35] which is based on highly detailed standardized finite element model (FEM) of the non-linear averaged anatomical template-ICBM152. The "New York Head" model has two different precision levels, corresponding to 74382 and 2004 voxels respectively. The dimension of lead field matrix we are using is 108×2004, representing 108 channels and 2004 voxels. We also assume that source orientation is perpendicular to the cortex surface. In Ref. [20] Sohrabpour et al. estimated source when source signal is around the peak value, similar practice can be found in Ref. [36]. As is shown in the experiment part of Ref. [37], the source images are plotted when the source activation is at peak value. Here in our experiments, we designed all the source activation magnitude bearing a positive value. For really EEG data, a technique called energy thresholding (in the following subsection) can be used to find the corresponding EEG data samples that have non-zero source activation pattern. In each simulation, noises originate from sensor level and cortex voxel level both contributed to the recorded EEG data. The SNR is calculated as

$$SNR = 20\log_{10}\frac{\|S\|_2}{\|N\|_2}.$$

The brain is divided into 8 Region Of Interest (ROI)s, namely RAI Right Anterior (RAI), Right Anterior Superior (RAS), Right Posterior Inferior (RPI), Right Posterior Superior (RPS), Left Anterior Inferior (LAI), Left Anterior Superior (LAS), Left Posterior Inferior (LPI), Left Posterior Superior (LPS) [38]. In the simulation experiments, we designed common sources that contain much higher magnitude and three discriminative sources related to three brain states with smaller magnitude from different ROIs. All computations in this paper were conducted on a 64–bit Linux workstation with i7-5960x CPU, memory of 64 GB and frequency being 3.00 GHz.

5.2 Validate the VOMP algorithm

In this subsection, we validated the VOMP under different SNR and source configurations. The voting threshold p was set to different values to test the VOMP's performance. For example, if we set the voting threshold to be 0.5, it means that a common source is determined when at least half of the samples in each class "agreed" the common source pattern. Note that, when there are more than 3 classes, the common source pattern is still extracted if more than 50% of at least 2 classes shared the same pattern. The VOMP algorithm can be further improved by using multi-step VOMP, which is to run OMP for multiple steps for each sample instead of just one step as described in Algorithm (2), and then aggregate the common source location information calculated from above steps and only keep the best one in terms of occurrences, and find the residual matrix and continue the VOMP procedure. Another improvement is that the spatially adjacent source locations can be regarded the same instead of treating them differently, as they have similar forward mappings.

The VOMP algorithm tries to reduce the signal correlation by decomposing common sources. Two experiments were conducted under different SNR values and source configurations. Each time, a different voting threshold was tested. In the first experiment, there are two common sources and two discriminative activated sources at different ROIs corresponding to three classes. Both noises originating from brain voxels and white noise from sensor measurement are added to the original signal. In the first experiment, the noise level is SNR= 17 dB. In the second experiment, the SNR is 12 dB with 3 common sources. The energy boxplots of 600 samples from 3 different classes under different voting threshold p are given in Fig.4. and Fig.5 for both experiment setups. The first common source can easily be extracted in the first iteration. However, if the noise level is large, it's hard to reach a consensus for a voting threshold $p = 0.3$ as is shown in Fig.5. Choose a small p will introduce false common source that will cause potential problem locating the right discriminative source. Our framework requires to check the accuracy and soundness of the final prediction and adjust the threshold back and forth. A recommended starting search point is $p = 0.2$. The advantage of VOMP is its speed as its core ingredient is OMP, and the evaluation time for each sample took 1.2763×10^{-4} s on our workstation. An example of our VOMP algorithm in filtering

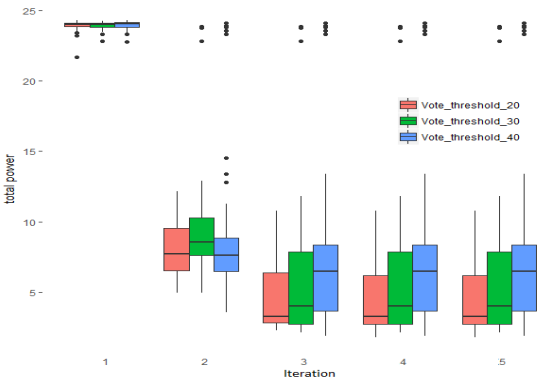

Fig. 4: Boxplot of total signal energy of 50 experiments: to show the effectiveness of VOMP in removal of common souces under SNR=17 with 2 common sources.

out the common background iteratively is illustrated in Fig.6, which is the time series version of "cross-and-bouquet" example,

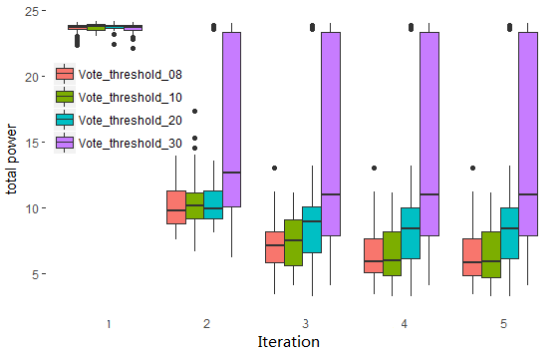

Fig. 5: Boxplot of total signal energy of 50 experiments: to show the effectiveness of VOMP in removal of common souces under SNR=12 with 3 common sources.

in contrast to the image recognition version as is illustrated in Fig.2 of Ref. [39].

5.3 Effect of Graph Regularization

In this section, we show the effectiveness of the graph regularization term in reconstructing the discriminative sources by comparing it with the other eight benchmark algorithms. We designed the spontaneous common sources with a magnitude of 0.8 with standard deviation to be 0.1 and task related discriminative source with a magnitude of 0.2 with a standard deviation of 0.05 located in different ROIs from the common sources.

We sampled 200 time points for each class and did the experiment 5 times to get the average accuracy of the reconstructed source. For the LGRDSR parameter, we set β to be 0.05 and α to be 0.06; M_{ij} is set to 1 if sample i and j belong to the same class since we care more about in-class consistency based on the example. The noise matrix is designed to affect the EEG recording together with the true source signal. For each time point, 3 random voxels are corrupted randomly with the average value being 0.2, 0.4, 0.6 and variance being 0.05 based on different SNR design. The 8 benchmark methods include ElasticNet [40], Homotopy [41], DALM [42], PDIPA [42], FISTA [42], sLORETA [11], MNE [7]. The former 6 algorithms are compared in image reconstruction applications and can be referred to Ref. [33] for details. The reconstruction performance of the proposed method as well as the benchmark methods based on 150 experiments are given in Table 1.

In Table 1, computation time is recorded in seconds (s), PSE represents primary source error, which is the distance of reconstructed primary source to the ground truth primary source. The distance evaluation is based on the shortest path of two voxels on the cortex surface instead of direct Euclidean distance. PSE measures the capability of each algorithm to reconstruct the common sources.

All of the values in Table (1), except the Time column in the table represents distance in (mm) from ground true source to the reconstructed source. When the reconstructed location is on a different hemisphere from the ground truth, there is no path connecting those two voxels, so we mark the distance to be 250 mm. EC1 represents error for class 1, which is the distance of the reconstructed discriminative source to the ground truth. EC2 and EC3 are similarly defined. To illustrate the effect of the proposed framework, the ground truth of the activated pattern is given in Fig.7, with the reconstructed source estimated by MNE, sLORETA, Homotopy, DALM and our method given in Fig.8–Fig.12. We can see from Table (1) and the Fig.8–Fig.12 that when the SNR is large, all the algorithms perform well in reconstructing primary sources. As for the discriminative sources for different classes, our method can achieve almost perfect reconstruction. All other algorithms' performances are also acceptable when SNR is large, except for sLORETA, MNE and ElasticNet. When we increase the noise, all of the algorithms can still achieve high accuracy in finding the primary source. For the discriminative source, our algorithm performs much better. We also validated that, to solve a pure ℓ_1 EEG inverse problem, the Homotopy algorithm performs better in most cases than other algorithms in the EEG inverse problem, which is in accordance with Ref. [33].

5.4 Discussion on Tuning the Parameters

Usually, if there are two parameters, the common practice is to do a grid search and find the best combination with the best performance. However, this can involve a lot of computation to find the best parameters. Moreover, the performance measurement can be misleading since it's not a direct measurement of accuracy, which is based on squared error of the reconstructed signal and the ground truth signal. Instead, it's based on the shortest path distance between inferred location and true source location. For example, if the ground truth signal is $(1, 0, 0, 0)$, the first reconstructed signal is $(0, 1, 0, 0)$, and the second reconstructed signal is $(0.3, 0, 0.7, 0)$, with the assumption that the neighboring elements in the vector are also neighboring voxels in the brain, the first reconstruction has larger squared error compared to the second one, even though the first one has better performance (location) precision. If the reconstructed sources are spurious ones (can be anywhere inside the brain), a better performance doesn't really mean the parameter setting is better compared to a worse performance in one numerical experiment. It may mean the spurious source with better accuracy happened to locate a source close to the actual source.

Based on the discussion above, its quite tricky to find the best combination of parameters. However, there are some ways to fine-tune the parameters. We propose a two-step fine-tuning mechanism. In the first step, we assign the graph regularization weight β to 0 and try to solve the simple ℓ_1 constrained problem using the Homotopy algorithm and find the best setting of α, which is quite easy since there is only one parameter to tune. The second step is to find the best value of β while fixing α. The rationale behind this is that our proposed model works well if the ℓ_1 problem can be solved with accurately. The graph regularization term can smooth out spurious sources that are not shared within a class, and the representative sources are encouraged and remained. The localization error under a different parameter setting is illustrated in Fig.13 under SNR = 16. Fig.13 is based on a result from 3rd outer iterations depicted in Algorithm (1). The inner maximum iteration is set to be 50. We assigned 250 mm when the inferred location is on a different hemisphere for visualization purposes. When the parameters are not well set, the graph penalty term will drive all the inferred source location from all time points to the wrong hemisphere. When the sparse regularization parameter α is set to be large, the solution will be a zero matrix.

5.5 Signal Energy Thresholding

In our experiments, we designed our primary sources to hold a large value, and the magnitude of discriminative sources are

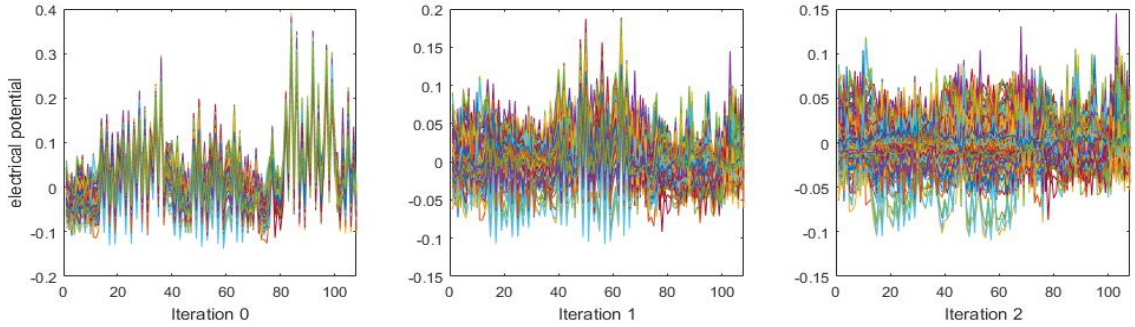

Fig. 6: Time series plot of common source decomposition: from left to right, common sources are removed iteratively.

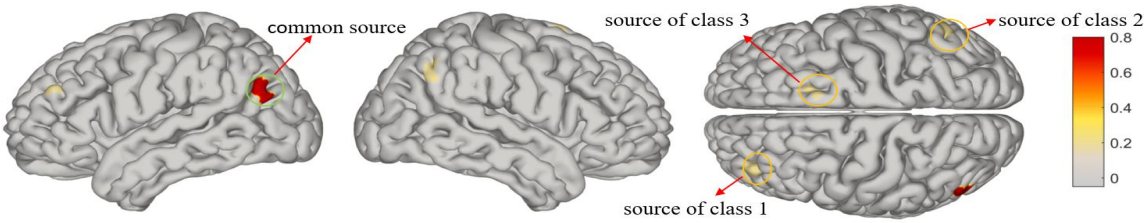

Fig. 7: Ground truth for all 3 classes

TABLE 1: Reconstruction Accuracy Summary

	SNR = 10					SNR =16					SNR = 22				
Methods	Time	PSA	EC1	EC2	EC3	Time	PSA	EC1	EC2	EC3	Time	PSA	EC1	EC2	EC3
ElasticNet [40]	0.001	43.4	142.3	159.6	159.2	0.001	21.5	188	162.3	136.0	0.001	8.87	172.5	195.0	13.0
Homotopy [41]	0.12	3.43	53.2	42.5	40.8	0.11	0.006	20.9	23.4	45.9	0.09	0	0.28	0.70	8.00
DALM [42]	0.07	4.59	53.0	43.1	39.6	0.07	0.01	20.9	22.0	45.5	0.08	0	0.28	1.73	7.98
PDIPA [42]	0.29	3.43	53.4	45.0	40.4	0.31	0.006	22.1	26.7	48.4	0.26	0	0.28	0.63	7.98
L1LS [42]	3.89	0.69	51.6	67.4	37.1	3.98	0.25	24.6	24.0	47.1	3.92	0.069	0	0	4.36
FISTA [43]	0.95	0.63	61.0	95.2	47.6	0.95	2.92	44.1	33.1	62.9	0.96	40.1	66.1	73.5	54.5
sLORETA [11]	0.015	10.2	131.7	178.2	142.8	0.015	16.9	200	175.1	152.1	0.02	2.62	194.1	164.2	123.5
MNE [7]	3e-5	29.3	131.8	157.7	131.7	3e-5	9.02	197.5	174.9	131.9	3e-5	4.30	119.8	136.2	113.5
LGRDSR	0.15	1.85	14.4	4.13	3.67	0.13	0.006	0	5.42	10.2	0.10	0	0	0	2.12

also larger than zero. One may argue that it's not realistic since the value we designed is never close to zero in real situations. However, the logic behind it is that once the source signal is close to zero, its contribution to the EEG data can't be reflected, making the corresponding reconstruction impossible. A useful technique to circumvent this problem is using Energy Thresholding (ET) of the EEG data. The purpose of ET is to eliminate data points of low energy with the hope of inferring a source signal that is not close to zero. The relationship between EEG data and source is $x_i = Ls_i + \epsilon$. Energy of the signal is defined as $p(x_i) = x_i^T x_i$. To find out the relationship of $p(x_i)$ and $p(s_i)$, we did a linear regression to predict $p(x_i)$ using $p(s_i)$ based on Monte Carlo simulation with 3000 samples, and found the linear trend between $p(x_i)$ and $p(s_i)$ is statistically significant, and the detailed regression model is given in Table (2).

TABLE 2: Regression result on energy of signal and source

	Estimate Std.	Error	t value	Pr($>|t|$)
(Intercept)	0.004841	0.008742	0.554	0.58
x	0.144889	0.007761	18.669	2e-16

From previous research, the Event-related potential demonstrates higher energy on P1 and N1 points that can be used to do the source mapping [44]. By using ET techniques, we can select the EEG data points with higher energy that correspond to source signals with higher energy. The discussion above shows it's reasonable to set the source signal with a magnitude not close to zero.

6 Conclusion and Future Research

In this paper, we proposed using label information to retrieve discriminative sources corresponding to different brain statuses, extending the traditional EEG source imaging problem to a supervised one guided by label information. Although determining a sparse representation with graph regularization in the computer vision and compressive sensing communities is not new, its application in the EEG inverse problem that implicitly utilizes label information has never been proposed. Our model employed a Laplacian graph regularized term that can boost the in-class similarity and discourage the out-class similarity, thus making the source solution from the same class more robust to noise. Numerical results show the proposed algorithm outperforms 8 benchmark algorithms in localizing the task related sources under certain levels of noise. We showed the common source decomposition using the "cross-and-bouquet" model in the inverse problem and presented an efficient algorithm to address the high background spontaneous source signals. Our proposed supervised version of EEG source imaging algorithm can be incorporated with other state-of-the-art algorithms, and an exemplary model called SVB-

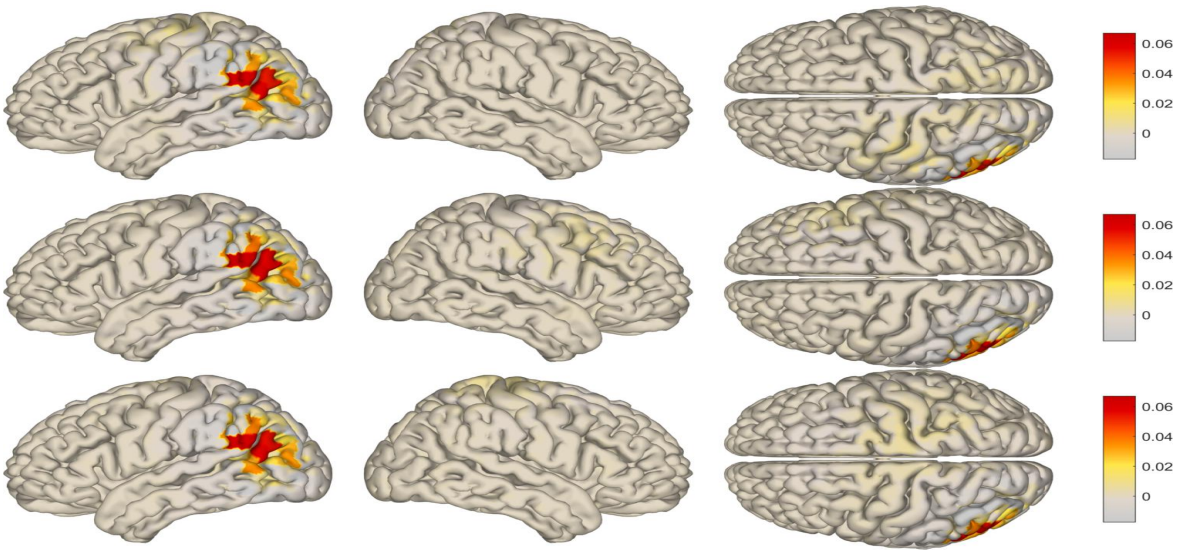

Fig. 8: MNE solution: The above row is the MNE solution for class 1; Class 2 and class 3 is illustrated in the middle and bottom row. The solution MNE gives is not sparse, with too many spurious sources of small magnitude.

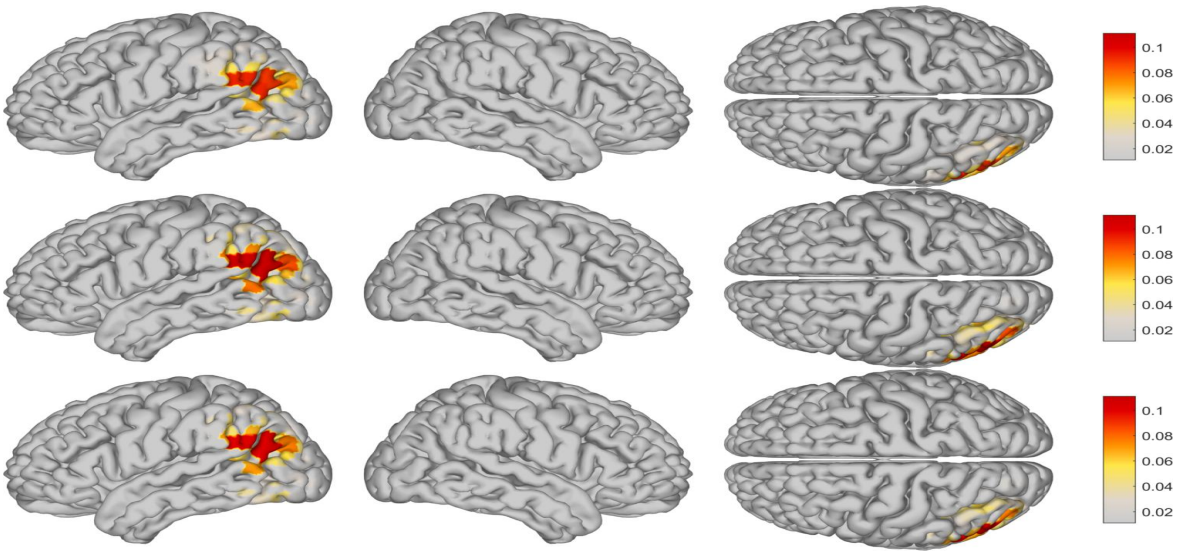

Fig. 9: sLORETA inverse solution: sLORETA solution for class 1, class 2 and class 3 is illustrated from the top to bottom rows. sLORETA can successfully reconstruct the primary source, however the secondary source is not successfully reconstructed. Compared to the solution of MNE, sLORETA can suppress the numerous spurious sources with small magnitude.

SCCD is demonstrated in our framework. The SVB-SCCD model is a special case of our proposed graph regularized one when the coefficient of the graph regularization term is zero. The graph regularized SVB-SCCD can be solved using ADMM optimization techniques. To sum up, the EEG inverse problem can be solved in a supervised framework, and it's beneficial to formulate it in that way to extract task related source activation patterns.

We tried to mimic the true source activation data using the simulated data. As it is well studied using fMRI data, our brain contains a resting state default mode network with some spontaneous neural behavior in certain brain areas. Another fact is that when given a specific task, different brain regions can be activated which correspond to the discriminative sources described in our paper. In that perspective, our model is more realistic than numerous previous studies that used simulated data. However, the weakness of our paper is that we used one spot as a common activated source, even though there may be several common source activation regions co-existing in reality. Overcoming this weakness is one of our future research goals.

Acknowledgments

This work been partially supported by the NSF funding under grant number CMMI-1537504 and DMS-1522786. The authors are also grateful to Dr. Stefan Haufe and Dr. Yu Huang for providing the head model. Thanks also give to Mr. Chunting Zhang, Mr. Aditya Amit Sheth for their proofreading.

References

[1] C. M. Michel, M. M. Murray, G. Lantz, S. Gonzalez, L. Spinelli, and R. G. de Peralta, "EEG source imaging," *Clinical neurophysiology*, vol. 115, no. 10, pp. 2195–2222, 2004.

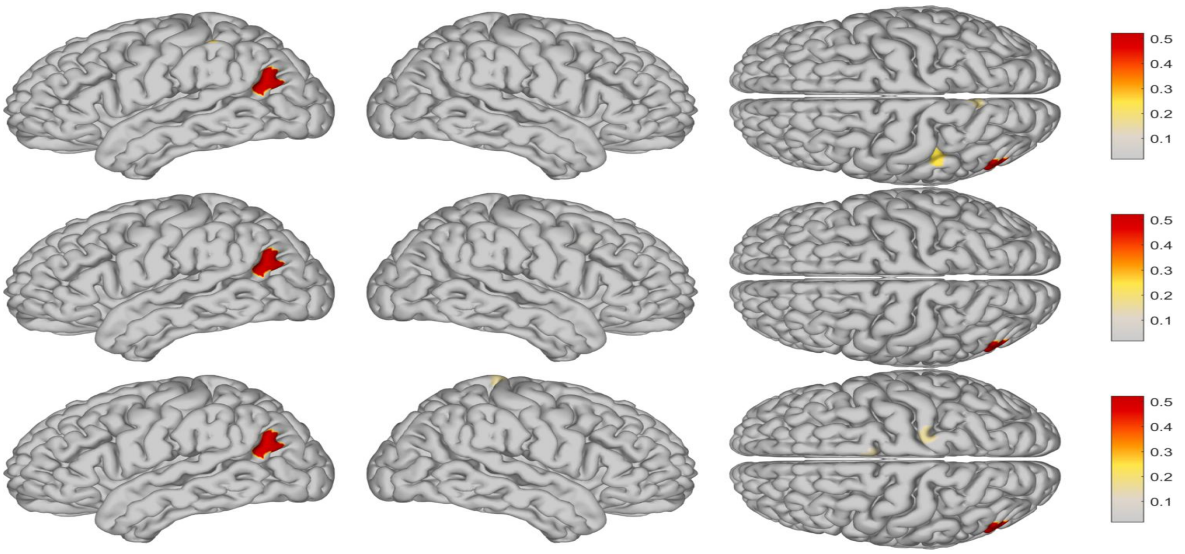

Fig. 10: Homotopy inverse solution: From top to bottom are the Homotopy solution for class 1, Class 2 and class 3 respectively. Homotopy can successfully reconstruct the primary source, however the secondary source is not successfully reconstructed. Compared to the solution of MNE and sLORETA, the solution is better in terms of accuracy and sparsity.

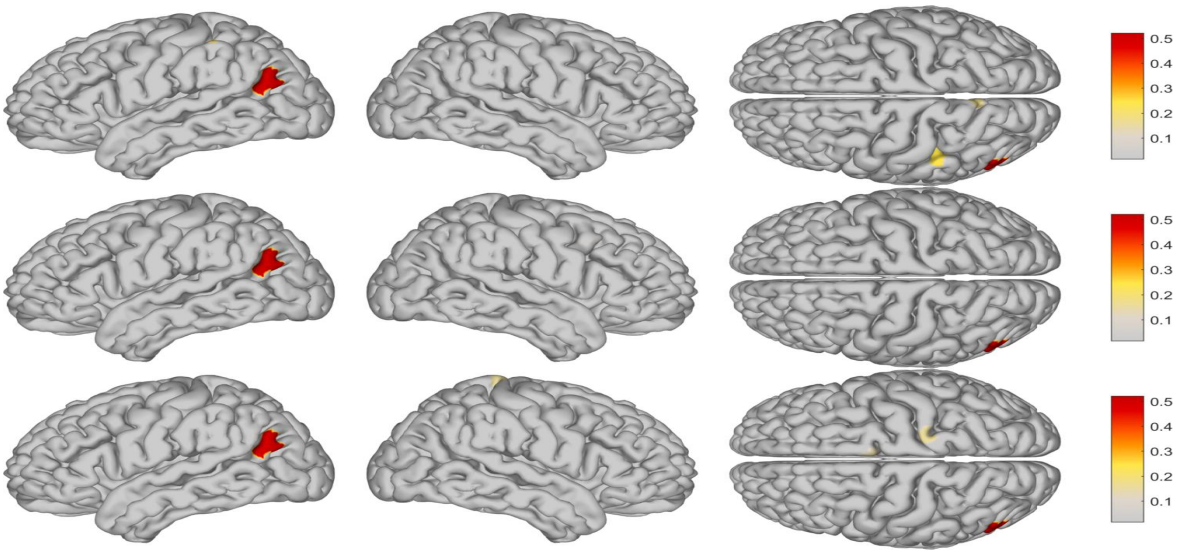

Fig. 11: DALM inverse solution: DALM can successfully reconstruct the primary source, however the secondary source is not successfully reconstructed. Compared to the solution of MNE and sLORETA, the solution is better in terms of accuracy and sparsity, similar performance compared to Homotopy.

[2] S. Haufe, V. V. Nikulin, A. Ziehe, K.-R. Müller, and G. Nolte, "Combining sparsity and rotational invariance in EEG/MEG source reconstruction," *NeuroImage*, vol. 42, no. 2, pp. 726–738, 2008.

[3] J. Perrier, P. Clochon, F. Bertran, C. Couque, J. Bulla, P. Denise, and M.-L. Bocca, "Specific EEG sleep pattern in the prefrontal cortex in primary insomnia," *PloS one*, vol. 10, no. 1, p. e0116864, 2015.

[4] J. Xiang, Y. Wang, Y. Chen, Y. Liu, R. Kotecha, X. Huo, D. F. Rose, H. Fujiwara, N. Hemasilpin, K. Lee *et al.*, "Noninvasive localization of epileptogenic zones with ictal high-frequency neuromagnetic signals: Case report," *Journal of Neurosurgery: Pediatrics*, vol. 5, no. 1, pp. 113–122, 2010.

[5] A. Sohrabpour, Y. Lu, P. Kankirawatana, J. Blount, H. Kim, and B. He, "Effect of eeg electrode number on epileptic source localization in pediatric patients," *Clinical Neurophysiology*, vol. 126, no. 3, pp. 472–480, 2015.

[6] X. Lei, T. Wu, and P. A. Valdes-Sosa, "Incorporating priors for EEG source imaging and connectivity analysis," *Frontiers in neuroscience*, vol. 9, 2015.

[7] M. S. Hämäläinen and R. J. Ilmoniemi, "Interpreting magnetic fields of the brain: minimum norm estimates," *Medical & biological engineering & computing*, vol. 32, no. 1, pp. 35–42, 1994.

[8] J. C. Mosher and R. M. Leahy, "Recursive music: a framework for EEG and meg source localization," *IEEE Transactions on Biomedical Engineering*, vol. 45, no. 11, pp. 1342–1354, 1998.

[9] ——, "Source localization using recursively applied and projected (rap) music," *IEEE Transactions on signal processing*, vol. 47, no. 2, pp. 332–340, 1999.

[10] R. D. Pascual-Marqui, D. Lehmann, T. Koenig, K. Kochi, M. C. Merlo, D. Hell, and M. Koukkou, "Low resolution brain electromagnetic tomography (LORETA) functional imaging in acute, neuroleptic-naive, first-episode, productive schizophrenia," *Psychiatry Research: Neuroimaging*, vol. 90, no. 3, pp. 169–179, 1999.

[11] R. D. Pascual-Marqui *et al.*, "Standardized low-resolution brain electromagnetic tomography (sloreta): technical details," *Methods Find Exp Clin Pharmacol*, vol. 24, no. Suppl D, pp. 5–12, 2002.

[12] I. F. Gorodnitsky, J. S. George, and B. D. Rao, "Neuromagnetic source imaging with focuss: a recursive weighted minimum norm algorithm," *Electroencephalography and clinical Neurophysiology*, vol. 95, no. 4,

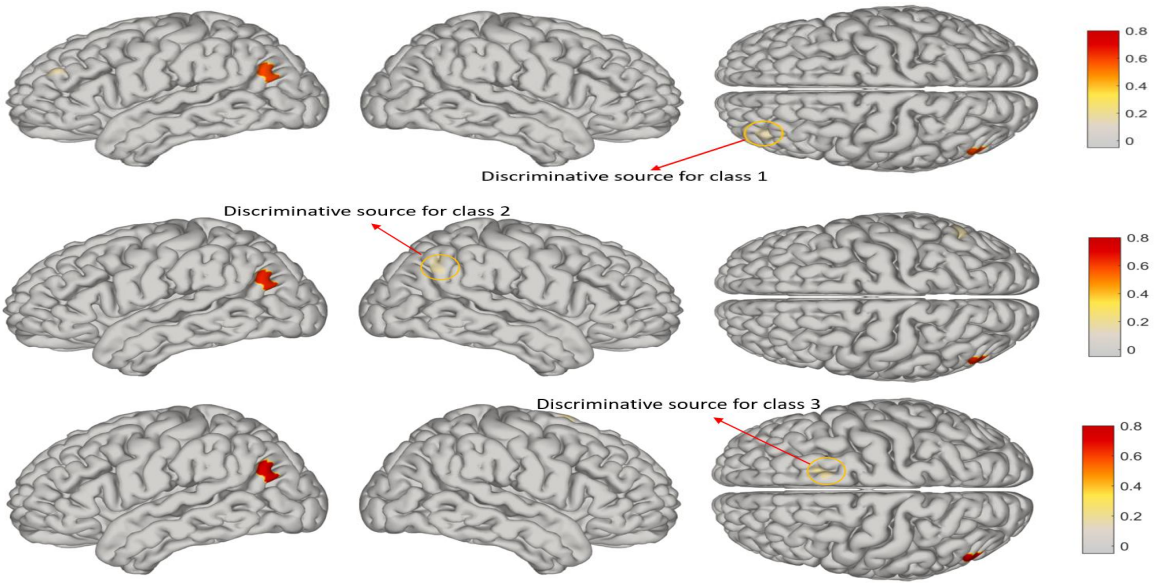

Fig. 12: LGRDSR reconstructed source: The reconstruction solutions for 3 classes are given in each row. As can be seen from the illustration, the discriminative source can be successfully reconstructed compared to other methodologies.

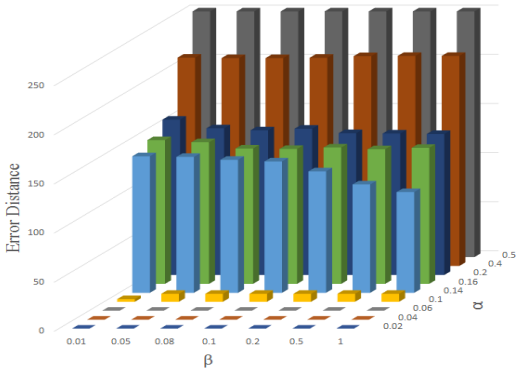

Fig. 13: Discriminative source location error (in mm) given different parameter settings

pp. 231–251, 1995.

[13] C. Song, T. Zhuang, and Q. Wu, "Hybrid weighted minimum norm method a new method based loreta to solve EEG inverse problem," in *2005 IEEE Engineering in Medicine and Biology 27th Annual Conference*. IEEE, 2006, pp. 1079–1082.

[14] C. Lamus, M. S. Hämäläinen, S. Temereanca, E. N. Brown, and P. L. Purdon, "A spatiotemporal dynamic distributed solution to the meg inverse problem," *NeuroImage*, vol. 63, no. 2, pp. 894–909, 2012.

[15] F. Costa, H. Batatia, L. Chaari, and J.-Y. Tourneret, "Sparse EEG source localization using bernoulli laplacian priors," *IEEE Transactions on Biomedical Engineering*, vol. 62, no. 12, pp. 2888–2898, 2015.

[16] A. Gramfort, M. Kowalski, and M. Hämäläinen, "Mixed-norm estimates for the M/EEG inverse problem using accelerated gradient methods," *Physics in medicine and biology*, vol. 57, no. 7, p. 1937, 2012.

[17] D. Strohmeier, Y. Bekhti, J. Haueisen, and A. Gramfort, "The iterative reweighted mixed-norm estimate for spatio-temporal MEG/EEG source reconstruction," *IEEE transactions on medical imaging*, vol. 35, no. 10, pp. 2218–2228, 2016.

[18] P. Xu, Y. Tian, X. Lei, and D. Yao, "Neuroelectric source imaging using 3sco: A space coding algorithm based on particle swarm optimization and l 0 norm constraint," *NeuroImage*, vol. 51, no. 1, pp. 183–205, 2010.

[19] Y. Li, J. Qin, Y.-L. Hsin, S. Osher, and W. Liu, "s-SMOOTH: Sparsity and smoothness enhanced EEG brain tomography," *Frontiers in Neuroscience*, vol. 10, p. 543, 2016.

[20] A. Sohrabpour, Y. Lu, G. Worrell, and B. He, "Imaging brain source extent from EEG/MEG by means of an iteratively reweighted edge sparsity minimization (ires) strategy," *NeuroImage*, vol. 142, pp. 27–42, 2016.

[21] L. Ding, "Reconstructing cortical current density by exploring sparseness in the transform domain," *Physics in Medicine and Biology*, vol. 54, no. 9, p. 2683, 2009.

[22] M. Zhu, W. Zhang, D. L. Dickens, and L. Ding, "Reconstructing spatially extended brain sources via enforcing multiple transform sparseness," *NeuroImage*, vol. 86, pp. 280–293, 2014.

[23] J. F. Hipp, D. J. Hawellek, M. Corbetta, M. Siegel, and A. K. Engel, "Large-scale cortical correlation structure of spontaneous oscillatory activity," *Nature neuroscience*, vol. 15, no. 6, pp. 884–890, 2012.

[24] M. E. Raichle, "The brain's dark energy," *Science*, vol. 314, no. 5803, pp. 1249–1250, 2006.

[25] D. L. Donoho, "For most large underdetermined systems of linear equations the minimal 1-norm solution is also the sparsest solution," *Communications on pure and applied mathematics*, vol. 59, no. 6, pp. 797–829, 2006.

[26] H. Guo, Z. Jiang, and L. S. Davis, "Discriminative dictionary learning with pairwise constraints," in *Asian Conference on Computer Vision*. Springer, 2012, pp. 328–342.

[27] D. Cai, X. He, J. Han, and T. S. Huang, "Graph regularized nonnegative matrix factorization for data representation," *IEEE Transactions on Pattern Analysis and Machine Intelligence*, vol. 33, no. 8, pp. 1548–1560, 2011.

[28] H. Lee, A. Battle, R. Raina, and A. Y. Ng, "Efficient sparse coding algorithms," in *Advances in neural information processing systems*, 2006, pp. 801–808.

[29] X. Lu, H. Yuan, P. Yan, Y. Yuan, and X. Li, "Geometry constrained sparse coding for single image super-resolution," in *Computer Vision and Pattern Recognition (CVPR), 2012 IEEE Conference on*. IEEE, 2012, pp. 1648–1655.

[30] M. A. Woodbury, "Inverting modified matrices," *Memorandum report*, vol. 42, p. 106, 1950.

[31] H. Becker, L. Albera, P. Comon, R. Gribonval, and I. Merlet, "Fast, variation-based methods for the analysis of extended brain sources," in *Signal Processing Conference (EUSIPCO), 2014 Proceedings of the 22nd European*. IEEE, 2014, pp. 41–45.

[32] J. Wright, Y. Ma, J. Mairal, G. Sapiro, T. S. Huang, and S. Yan, "Sparse representation for computer vision and pattern recognition," *Proceedings of the IEEE*, vol. 98, no. 6, pp. 1031–1044, 2010.

[33] A. Y. Yang, S. S. Sastry, A. Ganesh, and Y. Ma, "Fast ℓ 1-minimization algorithms and an application in robust face recognition: A review," in *Image Processing (ICIP), 2010 17th IEEE International Conference on*. IEEE, 2010, pp. 1849–1852.

[34] S. Boyd, N. Parikh, E. Chu, B. Peleato, and J. Eckstein, "Distributed optimization and statistical learning via the alternating direction method

of multipliers," *Foundations and Trends in Machine Learning*, vol. 3, no. 1, pp. 1–122, 2011.
[35] Y. Huang, L. C. Parra, and S. Haufe, "The new york head -a precise standardized volume conductor model for EEG source localization and tes targeting," *NeuroImage*, vol. 140, pp. 150 – 162, 2016, transcranial electric stimulation (tES) and Neuroimaging.
[36] H. Liu, P. H. Schimpf, G. Dong, X. Gao, F. Yang, and S. Gao, "Standardized shrinking LORETA-FOCUSS (SSLOFO): a new algorithm for spatio-temporal EEG source reconstruction," *IEEE Transactions on Biomedical Engineering*, vol. 52, no. 10, pp. 1681–1691, 2005.
[37] W. Ou, M. S. Hämäläinen, and P. Golland, "A distributed spatio-temporal EEG/MEG inverse solver," *NeuroImage*, vol. 44, no. 3, pp. 932–946, 2009.
[38] S. Haufe and A. Ewald, "A simulation framework for benchmarking EEG-based brain connectivity estimation methodologies," *Brain topography*, pp. 1–18, 2016.
[39] J. Wright and Y. Ma, "Dense error correction via ℓ^1-minimization," *IEEE Transactions on Information Theory*, vol. 56, no. 7, pp. 3540–3560, 2010.
[40] M. Vega-Hernández, E. Martínez-Montes, J. M. Sánchez-Bornot, A. Lage-Castellanos, and P. A. Valdés-Sosa, "Penalized least squares methods for solving the EEG inverse problem," *Statistica Sinica*, pp. 1535–1551, 2008.
[41] M. S. Asif and J. Romberg, "Sparse recovery of streaming signals using ℓ_1-homotopy," *IEEE Transactions on Signal Processing*, vol. 62, no. 16, pp. 4209–4223, 2014.
[42] Z. Zhang, Y. Xu, J. Yang, X. Li, and D. Zhang, "A survey of sparse representation: algorithms and applications," *IEEE access*, vol. 3, pp. 490–530, 2015.
[43] A. Beck and M. Teboulle, "A fast iterative shrinkage-thresholding algorithm for linear inverse problems," *SIAM journal on imaging sciences*, vol. 2, no. 1, pp. 183–202, 2009.
[44] S. Machado, O. Arias-Carrión, I. Sampaio, J. Bittencourt, B. Velasques, S. Teixeira, A. E. Nardi, R. Piedade, and P. Ribeiro, "Source imaging of p300 visual evoked potentials and cognitive functions in healthy subjects," *Clinical EEG and neuroscience*, pp. 262 – 268, 2014.

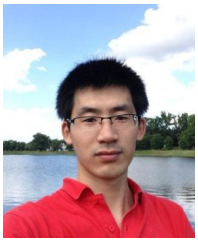

Feng Liu received the B.S. degree from Qingdao University, Qingdao, China in 2010 and the M.S degree in Huazhong University of Science and Technology (HUST), Wuhan, China in 2013, both Control Science and Engineering. Currently he is a PhD student majoring in industrial engineering in University of Texas at Arlington (UTA), TX, USA. His research interests include machine learning, EEG signal processing, brain imaging, sparse representation and chaos theory.

Jay Rosenberger Dr. Jay Rosenberger is a Professor of Industrial, Manufacturing, and Systems Engineering and Director of the Center on Stochastic Modeling, Optimization, & Statistics (COSMOS) at The University of Texas at Arlington (UTA). He has a B.S. in Mathematics from Harvey Mudd College, an M.S. in Industrial Engineering from the University of California at Berkeley, and a Ph.D. in Industrial Engineering from the Georgia Institute of Technology. His research interests include mathematical optimization and simulation in energy, transportation, defense, and health care. He is the President of the DFW Chapter of the INFORMS and the former chair and cluster chair of the INFORMS Health Applications Section. He has been a member of the Institute of Industrial Engineers since 2003.

Yifei Lou received the BS degree in Applied Mathematics from the Peking University in 2005 and the MS/Ph.D in Applied Mathematics from the University of California Los Angles in 2007 and 2010, respectively. Since 2014, she has been on the faculty of the Mathematical Sciences Department in the University of Texas Dallas. Her research interests include compressive sensing and its applications, image analysis (medical imaging, hyperspectral, imaging through turbulence), and (nonconvex) optimization algorithms. She is a member of the Society for Industrial and Applied Mathematics (SIAM) and Association for Women in Mathematics (AWM).

Rahilsadat Hosseini Rahilsadat Hosseini received the B.S degree from Iran University of Science and Tech in industrial engineering with focus on systems planning and analysis, and received the M.S. degree in industrial engineering from the University of Iowa, Iowa City, IA, in 2012. She is currently PhD student doing research in the Center on Stochastic Modeling, Optimization, and Statistics, University of Texas at Arlington, Arlington, TX, USA. Her research interests include data mining, pattern discovery, statistical and mathematical modeling, time

Jianzhong Su Dr. Jianzhong Su is a professor and the Chair of Department of Mathematics, the University of Texas at Arlington. His research area is in applied mathematics related to computational neuroscience, optical diffusive tomography and mathematical biology.

Shouyi Wang received the B.S. degree in control science and engineering from Harbin Institute of Technology, Harbin, China, in 2003 and the M.S. degree in systems and control engineering from Delft University of Technology, Delft, the Netherlands, in 2005 and the Ph.D. degree in Industrial and Systems Engineering from Rutgers University, Piscataway, NJ in 2012. From 2011-2013, he was a research scientist in the Department of Industrial and Systems Engineering and the Integrated Brain Imaging Center at School of Medicine, University of Washington, Seattle. Currently, he is an Assistant Professor of Industrial and Manufacturing Systems Engineering at the University of Texas at Arlington, Arlington, TX. His current research interests include big data analytics, data mining, machine learning, pervasive computing, healthcare/medical decision-making systems, multivariate time-series modeling and forecasting, real-time monitoring and early warning systems.